



Effect of Ion Exchange Times on the Morphology and Catalytic Activity of CoMn[Co(CN)₆] Film Catalyst in the Oxygen Evolution Reaction

Bui Thi Hoa^{1,*}, Vu Thi Kim Oanh², Pham Hong Hanh¹, Ngo Thi Anh Tuyet¹, Nguyen Thi Mai¹, Do Chi Linh¹, Nguyen Thi Giang¹, Nguyen Thanh Tung^{1,*}

¹ Institute of Materials Science, Vietnam Academy of Science and Technology, 18 Hoang Quoc Viet, Cau Giay, Hanoi, Vietnam

² Institute of Physic, Vietnam Academy of Science and Technology, 10 Dao Tan, Thu Le, Ba Dinh, Hanoi, Vietnam

* Email: hoabt@ims.vast.ac.vn; tungnt@ims.vast.ac.vn

ARTICLE INFO

Received: 29/03/2024

Accepted: 04/09/2024

Published: 30/06/2025

Keywords:

Hydrogen energy;
 CoMn[Co(CN)₆] film;
 ion exchange method;
 oxygen evolution reaction.

ABSTRACT

Hydrogen is a clean and high-energy fuel with the potential to serve as an alternative to fossil fuels. Water splitting is a promising method for efficient and cost-effective hydrogen production. The Oxygen Evolution Reaction (OER) plays a crucial role in water splitting but presents challenges in terms of efficiency. Therefore, it is necessary to develop OER catalysts that are both cost-effective and stable for practical and large-scale hydrogen production. In this study, we fabricated CoMn[Co(CN)₆] (CoMnCNC) films on carbon paper surfaces using the ion exchange method with varying ion exchange times (1h, 2h, 3h). The structural morphology of the fabricated films was analyzed using Scanning Electron Microscopy (SEM), X-ray Diffraction (XRD), and Energy-Dispersive X-ray Analysis (EDX). Furthermore, the catalytic activity of the CoMn[Co(CN)₆] films with different ion exchange times was investigated, and they exhibited good catalytic activity for the OER, along with stability in an alkaline environment.

Introduction

Fossil fuels are currently causing significant environmental and climate issues. Hydrogen is a high-energy carrier that has attracted considerable attention as a potential alternative to fossil fuels [1,2]. Additionally, it produces no greenhouse gas emissions or harmful pollutants [3]. As the demand for sustainable energy sources increases, scientists are exploring efficient methods to produce hydrogen. Water splitting ($\text{H}_2\text{O} \rightarrow \text{H}_2 + \text{O}_2$), particularly through the process of electrolysis, has been considered a promising technique for cost-effective and environmentally friendly hydrogen generation [4,5]. In water splitting process, the Oxygen

Evolution Reaction (OER) ($2\text{H}_2\text{O} \rightarrow 4\text{e}^- + 4\text{H}^+ + \text{O}_2$) plays a critical role in the overall efficiency of this process. The OER involves multiple steps, including the electrochemical oxidation of water molecules to produce oxygen gas, along with the release of protons and electrons. However, the OER is known to be a sluggish and kinetically demanding reaction, which limits its efficiency and hinders the practical application of water splitting for hydrogen production [6,7]. To overcome the challenges associated with the OER and enable efficient large-scale hydrogen production, it is necessary to develop highly active and stable catalysts. Iridium (Ir) and ruthenium (Ru)-based catalysts are well-known for their excellent catalytic activity in the OER[8].

However, their scarcity and high price hinder their widespread adoption for large-scale applications. Therefore, researchers are actively exploring alternative catalyst materials that are more abundant, cost-effective, and demonstrate high activity and stability in the OER [6,9,10]. Transition metal-based catalysts are being researched as potential alternatives to reduce costs and promote sustainable hydrogen production. A variety of catalysts, including oxides, hydroxides, phosphides, and chalcogenides, have been investigated for the OER [11–13]. Additionally, nanostructuring, alloying, doping, and surface engineering techniques have been studied to modify and optimize the catalytic properties of these materials. These strategies aim to enhance intrinsic activity, promote charge transfer, improve electrolyte interaction, and mitigate catalyst degradation, ultimately leading to improved OER performance [14,15]. Among these, Prussian Blue analogues such as $\text{Ni}(\text{Fe}(\text{CN})_6)_2$, $\text{Co}_3[\text{Fe}(\text{CN})_6]_2$, $\text{Co}[\text{Co}(\text{CN})_6]$, $\text{Mn}[\text{Co}(\text{CN})_6]$,... has been raised as promising catalyst for OER due to the CN bonds that bridge metal ion centers to form a 3D structure, resulting in high surface area and tunable structures [16–18]. However, up to now, $\text{CoMn}[\text{Co}(\text{CN})_6]$ has not been reported for investigating catalyst activity for OER yet.

Therefore, in this work, we focus on fabricating $\text{CoMn}[\text{Co}(\text{CN})_6]$ ($\text{CoMnCNC}o$) films on carbon fiber paper (CFP) surfaces using the ion exchange method. By varying the ion exchange times, the influence of the ion exchange duration on the structural morphology and catalytic activity of the fabricated films are studied. The structural morphology of the $\text{CoMnCNC}o$ films are characterized using SEM, XRD and EDX. The catalytic activity of the $\text{CoMnCNC}o$ films with different ion exchange times are investigated and demonstrated good catalytic activity and stability for the OER in alkaline medium.

Experiment section

Preparation of $\text{CoMn}[\text{Co}(\text{CN})_6]$ ($\text{CoMnCNC}o$) films.

Fluorine-doped tin oxide-coated glass (FTO) and carbon fiber paper (CFP) were utilized as substrates. The CFP was used as the substrate for SEM, EDX, and electrochemical measurements. Because the high XRD peaks of CFP would make the XRD peaks of the synthesized film difficult to observe, FTO glass was employed as the substrate for XRD measurements.

The ($\text{CoMnCNC}o$) films are fabricated through a two-step process. In the first step, CoMn -hydroxycarbonate (CoMn-HC) thin films are synthesized by hydrothermal method. A mixture of 0.075M $\text{Co}(\text{NO}_3)_2 \cdot 6\text{H}_2\text{O}$, 0.025M

$\text{MnCl}_2 \cdot 4\text{H}_2\text{O}$, and 0.2M $\text{CO}(\text{NH}_2)_2$ is prepared in distilled water. Substrates is immersed vertically in above mixture and heated at 90°C for 5 hours. After cooling down, the obtained films is thoroughly washed and then dried at 50°C for 24 hours.

In the second step, $\text{CoMn}[\text{Co}(\text{CN})_6]$ ($\text{CoMnCNC}o$) films is synthesized using the ion exchange method. The CoMn-HC film obtained from the first step is immersed in 0.1M $\text{K}_3[\text{Co}(\text{CN})_6]$ and heated at 60°C for 1, 2, or 3 hours. The resulting samples are labeled as $\text{CoMnCNC}o$ -1h, $\text{CoMnCNC}o$ -2h, and $\text{CoMnCNC}o$ -3h, respectively.

Films characterizations

The morphology of the film was examined using a SEM (FE-SEM, HITACHI S-4800) with an operating voltage of 15kV. The chemical composition of the sample was determined using EDX which integrated with the FE-SEM. The crystal structure of synthesized sample was analyzed using XRD (Rigaku D/MAX 2600 V, $\text{Cu K}\alpha$; $\lambda = 0.15418$ nm) with a scanning rate of 3°/min.

Electrochemical measurements

The electrochemical measurements were studied using a standard three-electrode system with a Pt-wire as the counter electrode, an Ag/AgCl (3 M KCl) as the reference electrode, and the films deposited on a CFP substrate as the working electrode. Linear sweep voltammetry (LSV) was used to evaluate the electrocatalytic performance of the films on the OER in a 1.0 M KOH electrolyte, with a sweeping rate of 5 mVs⁻¹ in a potential window from 1.0 to 2V vs RHE (Reversible Hydrogen Electrode). The stability of the catalyst's OER activity in 1.0 M KOH electrolytes was tested by performing cyclic voltammetry (CV) measurements for 100 cycles in the voltage range of 1.1-1.7V vs RHE, with a scan rate of 25 mV/s. The experimental bias potential ($E_{\text{Ag}/\text{AgCl}}$) applied against the Ag/AgCl reference electrode was then converted to the RHE scale using the equation $E(\text{RHE}) = E_{\text{Ag}/\text{AgCl}} + 0.059\text{pH} + E_{\text{Ag}/\text{AgCl}}^0$, where $E_{\text{Ag}/\text{AgCl}}^0 = 0.21$ V at 25°C.

Results and discussion

The $\text{CoMn}[\text{Co}(\text{CN})_6]$ ($\text{CoMnCNC}o$) film was fabricated through a two-step process. In first step, urea slowly decomposed to form NH_4^+ , OH^- , and CO_2 (as shown in reaction 1). The generated CO_2 then reacted with OH^- to form carbonate ions (CO_3^{2-}) (as shown in reaction 2). Subsequently, the Mn^{2+} and Co^{2+} ions reacted with the carbonate ions (CO_3^{2-}) and OH^- to form CoMn hydroxycarbonate film, as reaction 3 [19]. In the second step, the CoMn hydroxycarbonate used as precursor

<https://doi.org/10.62239/jca.2025.026>

film was ion exchanged in a solution containing $K_3[Co(CN)_6]$, following reaction 4.

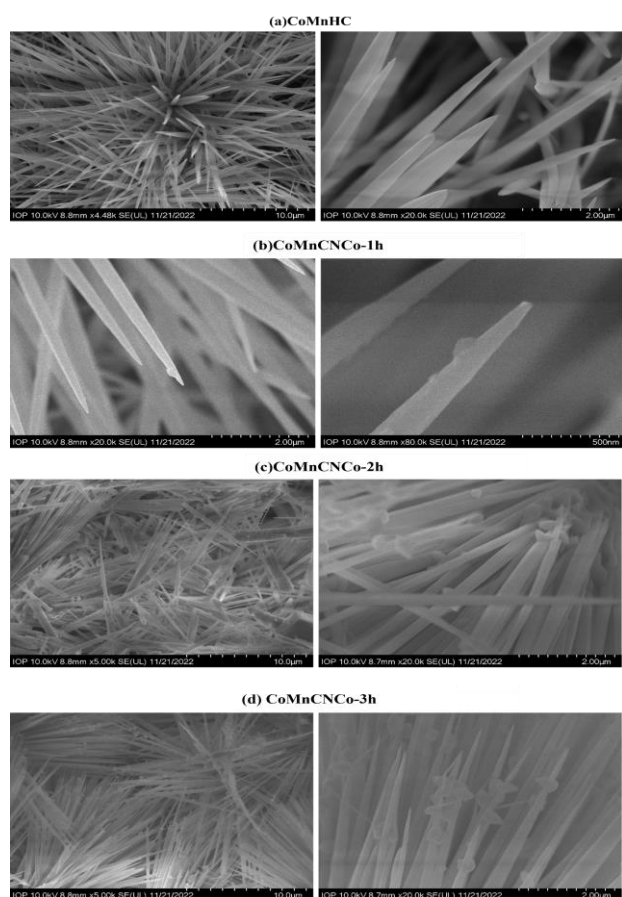
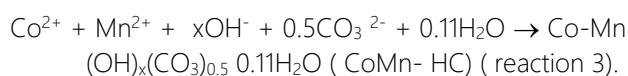
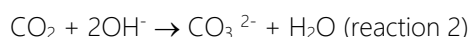
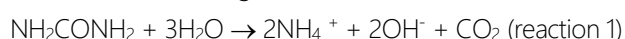


Figure 1: SEM images of (a) CoMn-HC; (b) CoMnCNC Co-1h; (c) CoMnCNC Co-2h and (d) CoMnCNC Co-3h on CFP.

The SEM surface images of the CoMn-HC, CoMnCNC Co-1h, CoMnCNC Co-2h, and CoMnCNC Co-3h films on the CFP substrate are presented in Figure 1 with two different magnifications. From the images, it is evident that the CoMnHC film exhibits nanoneedles structure. However, after undergoing ion exchange reaction with $K_3[Co(CN)_6]$, small particles can be observed growing on surface of the nanoneedles in Figures 1(b), (c), and (d). The amount of these particles increases with longer ion exchange durations, and their presence on the nanowire surface becomes more noticeable, as seen in Figure 1. Additionally, besides the increase in the number of particles on the nanoneedles, their size also gradually

increases during the ion exchange process. This combination of maintaining the nanoneedles structure while introducing additional particles is beneficial for enhancing the surface area of the catalyst material. It can improve catalytic activity and enhance the electrochemical properties of the synthesized material.

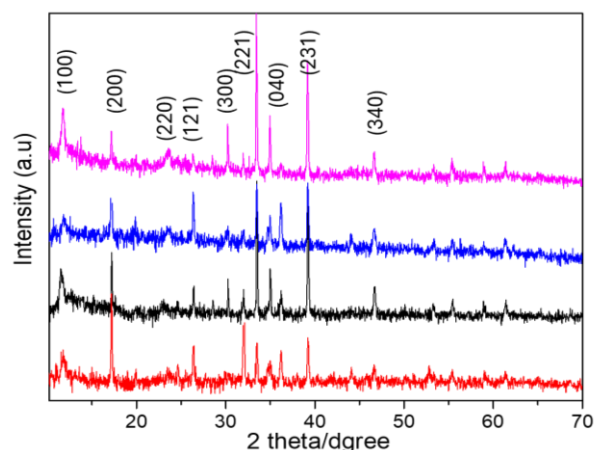


Figure 2: XRD patterns of CoMn-HC and CoMnCNC Co-1h; CoMnCNC Co-2h; CoMnCNC Co-3h on FTO glass.

Figure 2 illustrates XRD patterns of CoMn-HC and CoMnCNC Co-1h; CoMnCNC Co-2h; CoMnCNC Co-3h on FTO glass. After the ion exchange process to create CoMnCNC Co-1h, CoMnCNC Co-2h, and CoMnCNC Co-3h samples, new XRD peaks at angles of 23.65° , 28.48° , and 30.20° are observed corresponding to (220), (121), and (300) crystal planes respectively [20,21]. These new peaks gradually increased in width and intensity with longer ion exchange times, indicating it as the main peak of the CoMnCNC Co sample. It confirmed the successful synthesis of this compound using the ion exchange method [20,21]. Besides that, several diffraction peaks from the CoMn-HC film in the sample is remained as (100), (200), (221), (040), (231), and (340) crystal planes, although their intensity decreased, suggest the preservation of the nano-needle-like structure of the CoMnCNC Co films. The XRD results align with the SEM images, confirming the successful synthesis of CoMn[Co(CN) $_6$] films on a carbon paper surface through ion exchange with varying times.

Table 1: Atomic percentage of Mn, Co estimated from EDX spectra of CoMnCNC Co-1h; CoMnCNC Co-2h and CoMnCNC Co-3h samples.

Samples	Mn	Co
CoMnCNC Co-1h	2.7	24.93
CoMnCNC Co-2h	1.25	13.65
CoMnCNC Co-3h	2.18	24.80

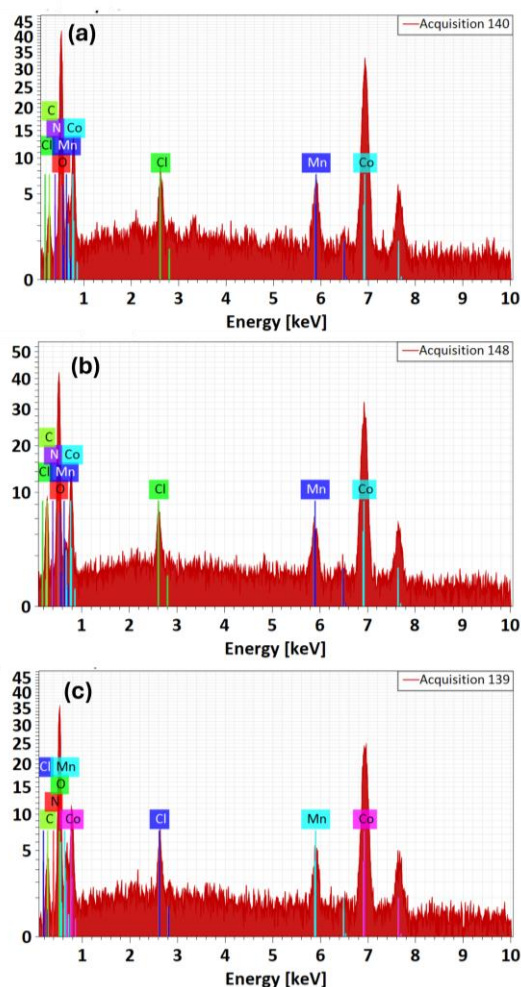


Figure 3: EDX spectra of CoMnCNCo-1h; CoMnCNCo-2h; and CoMnCNCo-3h films.

The EDX results for the CoMnCNCo-1h, CoMnCNCo-2h, and CoMnCNCo-3h samples are illustrated in Figure 3. To estimate the atomic percentages of Mn and Co in each sample, EDX spectra were analyzed, and the corresponding values are presented in Table 1. The spectra reveal the presence of Mn, Co, C, N, O, and Cl elements in the samples. Furthermore, the Co:Mn ratios for CoMnCNCo-1h, CoMnCNCo-2h, and CoMnCNCo-3h were determined to be 9.23:1, 10.92:1, and 11.37:1, respectively. This increase in the Co ratio can be attributed to the prolonged reaction time, which facilitates the gradual exchange and growth of $[\text{Co}(\text{CN})_6]^{3-}$ species from the solution onto the precursor films.

The CoMn-HC, CoMnCNCo-1h, CoMnCNCo-2h, and CoMnCNCo-3h films deposited on CFP were utilized as working electrodes, and their activity was investigated in OER in a 1 M KOH electrolyte. Figure 4 illustrates the LSV curves of the CoMn-HC, CoMnCNCo-1h, CoMnCNCo-2h, and CoMnCNCo-3h films during the OER in the 1 M KOH solution.

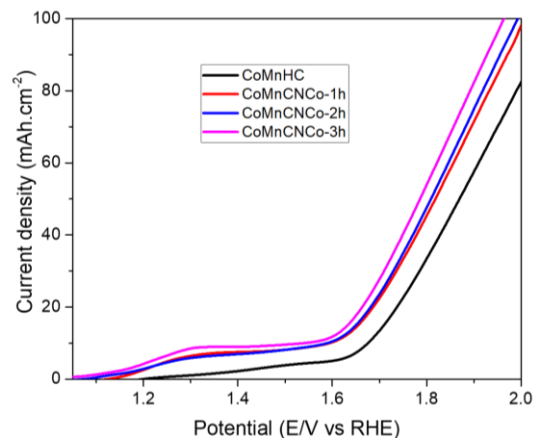


Figure 4: LSV curves of of CoMn-HC; CoMnCNCo-1h; CoMnCNCo-2h and CoMnCNCo-3h in OER in 1 M KOH electrolyte.

Upon ion exchange time to form CoMnCNCo-1h, CoMnCNCo-2h, and CoMnCNCo-3h films, these films exhibited higher catalyst activity compared to the CoMn-HC film. This can be attributed to the combined effect of an increased number of particles on the nanoneedles and their gradual size enlargement during the ion exchange process. These changes result in an expanded surface area of the catalyst material, which enhances its catalytic activity and improves its electrochemical properties. Furthermore, in the potential range of 1.2-1.6V vs. RHE, a broad peak is observed, indicating the oxidation/reduction processes taking place within the synthesized films. These processes involve the conversion of Co^{II} , Co^{III} , and Co^{IV} oxidation states within the dimeric Co redox centers: $\text{Co}^{\text{II}}\text{Co}^{\text{III}} \leftrightarrow \text{Co}^{\text{III}}\text{Co}^{\text{III}} \leftrightarrow \text{Co}^{\text{IV}}\text{Co}^{\text{III}} \leftrightarrow \text{Co}^{\text{IV}}\text{Co}^{\text{IV}}$ [22–24]. The characteristics of these peaks vary depending on the concentration of Co in the samples. Interestingly, the CoMnCNCo-3h film, which has a higher Co content, exhibits a larger peak within this voltage range. Moreover, when comparing the different ion exchange times of the samples, it is observed that the CoMnCNCo-3h film demonstrates the highest OER catalyst activity in an alkaline electrolyte, achieving a current density of 50 mA cm^{-2} at 1.77V. While, CoMnCNCo-2h film shows slightly lower activity at 1.80V, followed by the CoMnCNCo-1h film at 1.81V, and the CoMn-HC film at 1.87V to achieve a current density of 50 mA cm^{-2} . However, the differences in catalyst activity between the CoMnCNCo-1h, CoMnCNCo-2h, and CoMnCNCo-3h films are not significant. This may be due to the ratios of Co and Mn in these films are not significantly different, despite the varying ion exchange times of 1 hour, 2 hours, and 3 hours, as discussed in the EDX results.

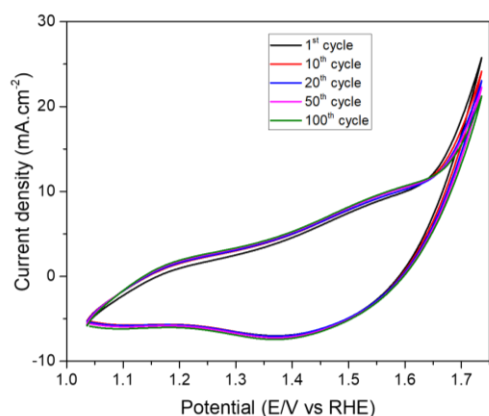


Figure 5: CV curves of CoMnCNCo-3h film in OER in the voltage window of 1.1V-1.7 V vs. RHE with 100 cycles

Moreover, the electrochemical stability of the synthesized CoMnCNCo-3h films was evaluated by conducting CV measurement for 100 cycles. Figure 5 displays the CV curves of CoMnCNCo-3h in the OER range of 1.1V-1.7V vs RHE. The results indicate that even after 100 cycles of CV, there is very little decrease and no change in the CV shape of the CoMnCNCo-3h film compared to the initial CV. This suggests that the CoMnCNCo-3h film displays exceptional stability for the oxygen evolution reaction in an alkaline 1M KOH electrolyte.

Conclusions

In this research, we successfully investigated the effect of ion exchange times on the morphology and catalytic activity of CoMn[Co(CN)₆] film catalyst in the oxygen evolution reaction. Varying the ion exchange times (1h, 2h, 3h) resulted in an increase in particle size and quantity on the nanoneedles, leading to an enhanced surface area of the catalyst material. The prolonged reaction time facilitated the gradual exchange and growth of [Co(CN)₆]³⁻ species onto the precursor films, increasing the Co ratio. Moreover, the CoMn[Co(CN)₆] catalysts with different ion exchange times exhibited good catalytic activity for OER and demonstrated stability in an alkaline environment.

Acknowledgment

This work is supported by Vietnam Academy of Science and Technology under grant number TĐHYD0.04/22-24.

References

1. L. Ge, B. Zhang, W. Huang, Y. Li, L. Hou, J. Xiao, Z. Mao, X. Li, *J. Energy Storage*, 75 (2024) 109307. <https://doi.org/10.1016/j.est.2023.109307>
2. U. Bossel, B. Eliasson, *Proc. Eur. Fuel Cell Forum, Lucerne*, 36 (2002). https://afdc.energy.gov/files/pdfs/hyd_economy_bosel_eliasson.pdf

<https://doi.org/10.62239/jca.2025.026>

3. J.O. Abe, A.P.I. Popoola, E. Ajenifuja, O.M. Popoola, *Int. J. Hydrogen Energy*, 44(44) (2019) 15072–15086. <https://doi.org/10.1016/j.ijhydene.2019.04.068>
4. J. Mohammed-Ibrahim, S. Xiaoming, X. Sun, *J. Energy Chem.*, 34 (2019) 111–160. <https://doi.org/10.1016/j.jechem.2018.09.016>
5. S. Li, E. Li, X. An, X. Hao, Z. Jiang, G. Guan, *Nanoscale*, 13(26) (2021) 12788–12817. <https://doi.org/10.1039/D1NR02592A>
6. K. Zhang, R. Zou, *Small*, 17 (2021) 2100129. <https://doi.org/10.1002/smll.202100129>
7. J. Song, C. Wei, Z.-F. Huang, C. Liu, L. Zeng, X. Wang, Z.J. Xu, *Chem. Soc. Rev.*, 49 (2020) 2196–2214. <https://doi.org/10.1039/C9CS00607A>
8. C.C.L. McCrory, S. Jung, I.M. Ferrer, S.M. Chatman, J.C. Peters, T.F. Jaramillo, *J. Am. Chem. Soc.*, 137 (2015) 4347–4357. <https://doi.org/10.1021/ja510442p>
9. M.-I. Jamesh, X. Sun, *R.J. Power Sources*, 400 (2018) 31–68. <https://doi.org/10.1016/j.jpowsour.2018.07.125>
10. R.R. Raja Sulaiman, W.Y. Wong, K.S. Loh, *Int. J. Energy Res.*, 46 (2022) 2241–2276. <https://doi.org/10.1002/er.7380>
11. Z. Cai, X. Bu, P. Wang, J.C. Ho, J. Yang, X. Wang, *J. Mater. Chem. A*, 7 (2019) 5069–5089. <https://doi.org/10.1039/C8TA11273H>
12. F. Wang, T.A. Shifa, X. Zhan, Y. Huang, K. Liu, Z. Cheng, C. Jiang, J. He, *Nanoscale*, 7 (2015) 19764–19788. <https://doi.org/10.1039/C5NR06718A>
13. X. Li, X. Hao, A. Abudula, G. Guan, *J. Mater. Chem. A*, 4 (2016) 11973–12000. <https://doi.org/10.1039/C6TA02334G>
14. Y. Jiao, Y. Zheng, M. Jaroniec, S.Z. Qiao, *Chem. Soc. Rev.*, 44 (2015) 2060–2086. <https://doi.org/10.1039/C4CS00470A>
15. G. Mohan Kumar, P. Ilanchezhian, C. Siva, A. Madhankumar, T.W. Kang, D.Y. Kim, *Int. J. Hydrogen Energy*, 45 (2020) 391–400. <https://doi.org/10.1016/j.ijhydene.2019.10.104>
16. H.T. Bui, D.Y. Ahn, N.K. Shrestha, M.M. Sung, J.K. Lee, S.H. Han, *J. Mater. Chem. A*, 4 (2016) 9781–9788. <https://doi.org/10.1039/C6TA03436E>
17. B. Singh, A. Indra, *Mater. Today Energy*, 16 (2020) 100404. <https://doi.org/10.1016/j.mtener.2020.100404>
18. L.M. Cao, D. Lu, D.C. Zhong, T.B. Lu, *Coord. Chem. Rev.*, 407 (2020) 213156. <https://doi.org/10.1016/j.ccr.2019.213156>
19. H.H. Pham, D.C. Linh, T.T.A. Ngo, V.T.K. Oanh, B.X. Khuyen, S.A. Patil, N.H.T. Tran, S. Park, H. Im, H.T. Bui, N.K. Shrestha, *Dalton Trans.*, 52 (2023) 12185–12193. <https://doi.org/10.1039/D3DT02426A>
20. L. Hu, P. Zhang, Q. Chen, N. Yan, J. Mei, *Dalton Trans.*, 40 (2011) 5557–5562. <https://doi.org/10.1039/C1DT10134J>
21. L. Yang, T. Qiu, M. Shen, H. He, H. Huang, *Compos. Sci. Technol.*, 196 (2020) 108232. <https://doi.org/10.1016/j.compscitech.2020.108232>
22. F. Wu, X. Guo, G. Hao, Y. Hu, W. Jiang, *J. Solid State Electrochem.*, 23 (2019) 2627–2637. <https://doi.org/10.1007/s10008-019-04362-x>
23. B. Sidhureddy, J.S. Dondapati, A. Chen, *Chem. Commun.*, 55 (2019) 3626–3629. <https://doi.org/10.1039/C8CC10194A>
24. F. Dionigi, Z. Zeng, I. Sinev, T. Merzdorf, S. Deshpande, M.B. Lopez, S. Kunze, I. Zegkinoglou, H. Sarodnik, D. Fan, A. Bergmann, J. Drnec, J.F. de Araujo, M. Gliach, D. Teschner, J. Zhu, W.-X. Li, J. Greeley, B.R. Cuenya, P. Strasser, *Nat. Commun.*, 11 (2020) 2522. <https://doi.org/10.1038/s41467-020-16237-1>